Iraqi Geological Journal

Journal homepage: https://www.igj-iraq.org

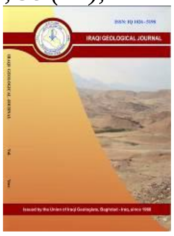

Characteristics of Limestone Outcrops Based on Landsat 8 Image and Geochemical Analysis in South Buton Regency, Southeast Sulawesi Province, Indonesia

Andi Fahdli Heriansyah[1], Citra Aulian Chalik[1*], and Muhamad Hardin Wakila[1]

[1] Department of Mining Engineering, Universitas Muslim Indonesia, Makassar, Indonesia

* **Correspondence**: citraaulian@umi.ac.id

Received: 19 September 2024
Accepted: 5 May 2025
Published: 31 July 2025

Abstract

Identification of limestone outcrops aims to determine the potential location, distribution, and quality of limestone. With advances in remote sensing technology, limestone identification can be carried out using Landsat 8 OLI satellite imagery data. This study aims to identify the characteristics of the limestone potential area with the Landsat 8 image processing method used is band ratio, color composite and normalized differential vegetation index. Each result of the Landsat 8 image processing method can show the characteristics and distribution of limestone outcrops based on color and spectral differences from Landsat 8 image data. Spectral analysis of Landsat 8 image data was carried out to see the reflectance level of each band which can show differences in unexposed limestone outcrops, or unmined and exposed or mined limestone. The normalized differential vegetation index method can show potential locations of limestone whose vegetation has been disturbed by mining activities. The chemical characteristics of limestone can be determined by geochemical testing of X-Ray Fluorescence limestone samples. Of geochemical analysis, X-Ray Fluorescence is carried out in the laboratory to determine the main chemical elements and trace elements of the rock. This research will help industrial engineers to explore the potential of limestone in south Buton.

Keywords: Limestone; Landsat-8; Band ratios; Colour composite; NDVI

1. Introduction

Limestone in the South Buton area is widespread and clearly exposed. One of the exposed limestone is the Rongi Hill, which is included in the reef limestone Wapulaka Formation. Southeast Sulawesi Province is one of the prospective areas for limestone exploration and mining. The area is marked by the existence of two mining business permit areas located in South Buton. As infrastructure, population, and regional development increase, the exploitation of limestone is increasingly supporting the government and society to meet infrastructure needs. Limestone is the primary raw material required for drainage and infrastructure (Soni and Nema, 2021).

Geological mapping is important for any geological work and provides vital information about the geology of the area, such information can be used for several proposes (Bety, 2022). Remote sensing is the initial method used for geological mapping that covers a large area. This method is inexpensive and time consuming for obtaining surface rock information (Abdelmalik, 2020). The rapid advancement of remote sensing techniques and technologies is increasingly beneficial to researchers across various disciplines. A significant use case can be found in geological studies, where these techniques are employed for mapping structural features and rock types, as well as identifying and locating

DOI: https://doi.org/10.46717/igj.2025.58.2A.1

economically significant mineral deposits (Amer et al., 2010; Gad, and Kusky, 2006). The processing of remote sensing data requires many algorithms and mathematics/statistics that have been developed and used to improve the interpretation of geological features/targets. In the fields of lithology mapping and mineral exploration, two techniques stand out as the most effective and widely used: band ratio and principal component analysis (PCA) (Abdelmalik, 2020; Bety et al., 2024). Spectral integration of remote sensing data from each studied target stands as the most crucial remote sensing technique. The spectral curve of remote-sensing data contains information that reveals the physical and chemical properties of each object, target, or rock under examination. Studies have demonstrated that the distinctive spectral patterns of rocks and minerals are produced by mechanisms linked to electron movement and transition (Hunt, 1977). The spectral signature of remote sensing data is influenced not only by the rock's chemical makeup but also by its physical characteristics, such as porosity and grain size (Hunt, 1977). The distribution of rocks and minerals on the surface was determined and interpreted using these characteristic spectral patterns (Salih, 2023)

The Landsat 8 OLI (Operational Land Imager) and TIRS (Thermal Infrared Sensor) were introduced in 2013, marking the recent enhancements to the Landsat satellite program. This iteration of Landsat features decreased bandwidth and incorporates two new spectral bands. Multiple studies have shown Landsat 8's capability in delineating geological structures and detecting zones of hydrothermal alteration (Benaissi et al., 2022; Lu et al., 2022, Osinowo et al., 2021; Salih, 2023), which show that the spectral data from the Landsat 8 band are very helpful in lithology mapping. Regional geological mapping was performed by Pour and Hashim (2011) utilizing Landsat 8 and ASTER satellite imagery, employing the band-ratio index technique. In lithology mapping, the textural characteristics of Landsat 8 images prove beneficial (Wei et al., 2016). In addition to the band ratio method, the color combination method can be used for geological mapping, as was done by Pour et al. (2018) for hydrothermal alteration mapping using Landsat 8 (Pour and Hashim, 2023).

Limestone mining locations usually experience land cover changes that impact long-term land and environmental conditions. The normalized differential vegetation index (NDVI) method can be used to assess changes in vegetation cover due to changes in land cover caused by active limestone mines. Venkata et al. (2022) used Landsat 8 to calculate the NDVI value to detect limestone mining locations and their impact on environmental changes (Venkata et al., 2022).

The research sought to evaluate limestone potential in South Buton, Southeast Sulawesi Province, utilizing Landsat 8 imagery through the application of band ratio, color combination, and NDVI techniques. This research was also carried out by field studies to obtain several limestone samples from locations that were not limestone mining locations and limestone samples from active or former limestone mining sites. Spectral analysis was performed to determine the reflection level of each band indicated by the limestone at the study site. This research is expected to yield results that will prove valuable to researchers, industry professionals, and the environment in the areas of limestone exploration and ecological conservation. By contributing to the development of eco-conscious mining sites, this study aims to promote long-term sustainability in the sector.

2. Materials and Methods

2.1. Study Area

The research area was the South Buton Regency, Southeast Sulawesi Province. The selected area is the Wapulaka Formation (QPW) , which is a limestone formation of algae and coral reefs. The age of formation is late Pliocene to Pleistocene and consists of bioclastic limestone (Sikumbang, 1995). The limestone in the study area is characterized by coastal steps that rise to the surface because the geology of the southern island of Buton is bordered by the Flores Sea (Fig. 1). Based on ESDM (Energy and

Mineral Resources) data at https://geoportal.esdm.go.id/minerba/, there are two limestone IUPs (Mining Business Permits) for industries located in South Buton Regency. The IUP remained in the exploratory stage. The research area was located at geographical coordinates 122°40' – 122°55' East Longitude and 5°25'-5°45' South Latitude.

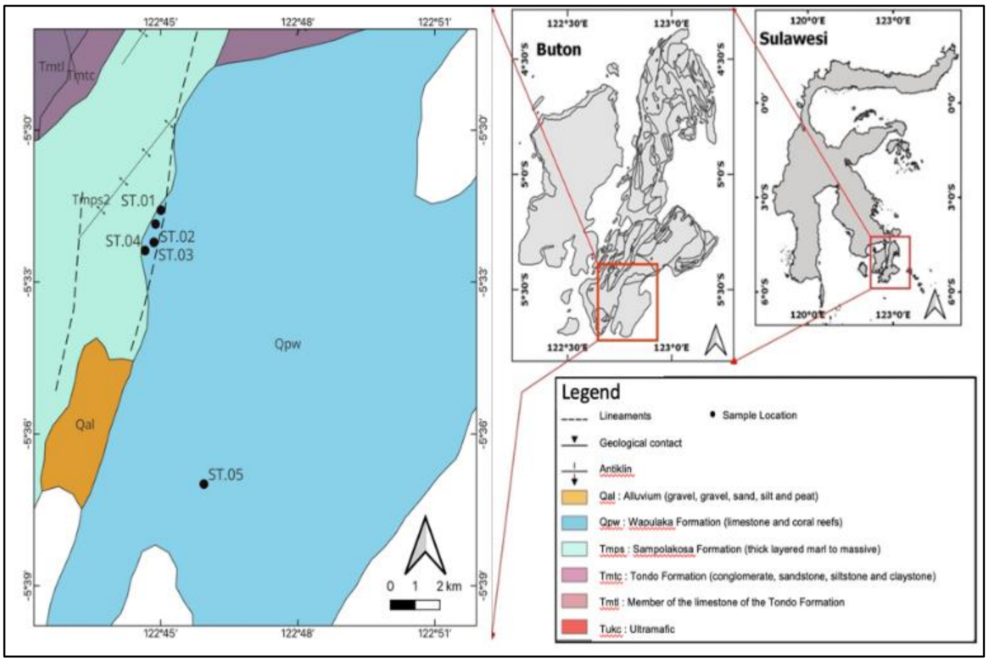

Fig. 1. Geological map of the study area in South Buton, Southeast Sulawesi province, with located of 5 field stations

2.2. Data

For this study, the geospatial information was acquired from the United States Geological Survey (USGS) Earth Explorer platform. This satellite features 11 bands, encompassing visible, infrared, and thermal ranges. Table 1 shows the spectral specifications and spatial resolution of the Landsat-8 OLI (Operational Land Imager). VNIR and SWIR bands have a spatial resolution of 30 m, while the thermal band has a resolution of 100 m. For limestone studies, the VNIR and SWIR bands are utilized to perform ratios, color composites, and NDVI calculations. This study employed Landsat 8 data from Path 112/ Row 64, captured on December 10, 2015. The imagery underwent geometric correction and georeferencing to the UTM (51 South Zone) projection using the WGS-84 datum.

Table 1. The Spectral Characteristics and Spatial Resolution of Landsat Band 8

	No Band	Wavelength (μm)	Spatial Resolution (m)	Band
VNIR	1	0,43-0,45	30	Ultra-Blue (Coastal/Aerosol)
	2	0,45-0,51		Blue
	3	0,53-0,59		Green
	4	0,64-0,67		Red
	5	0,85-0,88		NIR
	8	0,50-0,68	15	Panchromatic
SWIR	9	1,36-1,38	30	Cirrus
	6	1,57-1,65		SWIR 1
	7	2,11-2,29		SWIR 2
TIR	10	10,60-11,19	100	TIR 1
	11	11,50-12,51		TIR 2

2.3. Pre-Processing and Processing Landsat 8

This study employed Landsat 8 to examine limestone's spectral properties, colour composite, and Normalized Difference Vegetation Index (NDVI) values. This study also aims to show the ability of Landsat 8 to identify sensitive bands in limestone. and to create more interpretable images for limestone identification in the study area, these selected spectral bands were used in ratio calculations, composite color image generation, and NDVI computations. Before analyzing limestone presence with Landsat 8 data, it was crucial to conduct pre-processing steps using ENVI software, specifically focusing on radiometric and atmospheric corrections. This pre-processing phase eliminated atmospheric interference effects, yielding more accurate measurements of reflectivity, emissivity, surface physical properties, and surface temperature (Muchsin et al., 2018). The process of radiometric correction involves converting Digital Numbers (DN) to radians and/or reflectance, followed by atmospheric adjustment using the FLAASH (Fast Line-of-sight Atmospheric Analysis of Spectral Hypercubes) tool within ENVI software. Subsequently, the Landsat image is trimmed to match the study area's boundaries.

The band ratio, color composite, and NDVI processes are the next processes after data preprocessing is complete. This process is a technique for improving the image quality for clearer interpretation targets, especially for improving the image quality targets in limestone lithology mapping. In remote sensing analysis, the band ratio technique compares two spectral bands for a single color in the RGB (Red, Green, Blue) system, resulting in a specific rock surface appearance. Following this, a color composite process is employed, which combines three colors to map lithological zones. The final step in processing Landsat 8 imagery involves generating an NDVI (Normalized Difference Vegetation Index) map by applying the NDVI algorithm to the appropriate Landsat 8 image bands.

These techniques collectively enhance the visual interpretation of geological features and vegetation cover. The band ratio method highlights specific rock compositions, while color composites provide a comprehensive view of lithological variations. NDVI mapping further complements the analysis by quantifying vegetation density and distribution, which can indirectly inform about underlying geological conditions.

The next stage is to identify the chemical content of limestone samples taken in the field using X-Ray Fluorescence (XRF). The XRF analysis will provide detailed information on the elemental composition of the limestone, allowing for a more comprehensive understanding of its geological characteristics. This data can then be correlated with the Band Rasio (BR), Color Composite (CC) and NDVI mapping results to establish potential relationships between vegetation patterns and specific mineral content in the outcrop limestone. By integrating these multiple lines of evidence, researchers can develop a more robust model of the geological landscape and its influence on surface vegetation.

3. Results and Discussion

3.1. Band Rasio (BR)

The Band Ratio method is the remote sensing enhancement method applied in this study. The BR method enchances the contrast between targets or features based on dividing the reflectance for the one band pixels by the same picels in other band (Amer et al., 2010; Ding et al., 2014). This approach is particularly effective in identifying features or materials that are not easily discernible in the original band. Additionally, the band ratio transformation proves valuable in detecting minerals associated with hydrothermal alteration processes (Pour et al., 2011; Rockwell and Hofstra, 2008; Di Tomasso and Rubinstein, 2007).

Two band ratios for RGB images have been used for mapping lithology and hydrothermal alteration: Sabin ratios (4/2, 6/7, and band 10 as RGB and 4/2, 6/5, and 6/7 as RGB) (Sabins, 1999). The mineralized limestone spectrum shows high reflectance in band 6 Landsat 8 OLI and low reflectance in band 7, which is due to weak alteration of gypsum and clay. Therefore, the ratio (7/6) of Landsat 8 OLI can be used to extract mineralized limestone (Amer et al., 2010; Bedini, 2011). The two bands compared for each RGB color were chosen to better extract the lithological units. The ratios of the two bands used in this research to extract limestone were R5/4, G6/5, and B7/2, and the second band ratios used in this research were R6/5, G 7/6, and B 4/7 (Fig. 2). Fig. 2 shows color variations for unmined and mined limestone outcrops, in addition to colors for non-limestone or identified as forest or vegetation.

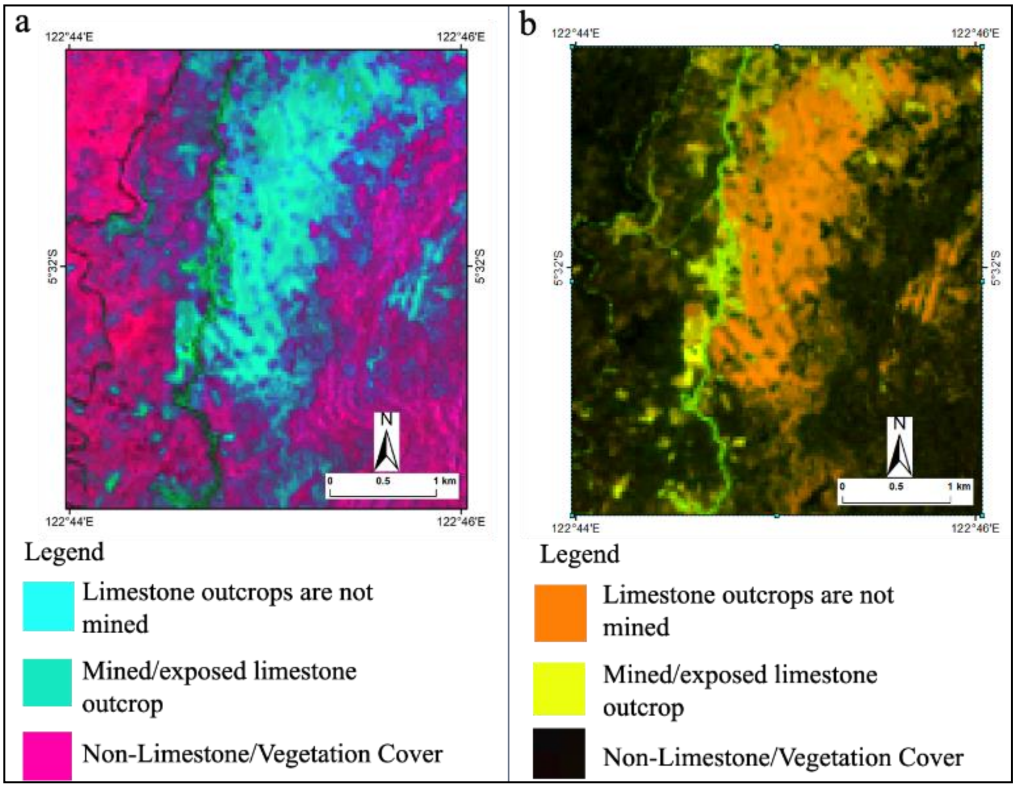

Fig. 2. (a) R5/4, G6/5, and B7/2 band ratio results; (b) R6/5, G7/6, and B 4/7 band ratio of Landsat 8

3.2. Color Composite (CC)

The generation of color composites depends on the spectral properties of modified rocks and minerals. Clay and carbonate minerals exhibit absorption features in the 2.1 to 2.4 μm range, while reflectance is noted between 1.5 and 1.7 μm (Ourhzif et al., 2019). Following an analysis of various band ratio combinations, two RGB color composite schemes were chosen to improve the detection of existing lithological units and mineralization areas (Amer et al., 2010; Crouvi et al., 2006; Moghtaderi and Zadeh, 2007; Di Tomasso and Rubenstein, 2007). Landsat 8 OLI employs bands R4, G3, and B2 for natural RGB color composites. This research utilized an RGB color composite of 753 to identify limestone (Fig. 3a). The wavelength ranges for these bands are: 2.11-2.29 µm for band 7 (SWIR 2), 0.85-0.88 µm for band 5 (Near Infrared), and 0.53-0.59 µm for band 3 (Green). Additionally, an alternative RGB color composite of 762 was used to detect limestone presence (Fig. 3b), band 7 (SWIR 2) has a wavelength of 2.11-2.29 µm, band 6 (SWIR 1) has a wavelength of 1.57-1.65 µm, and band 2 (Blue) has a wavelength of 0.45-0.51 µm (Heriansyah et al., 2022).

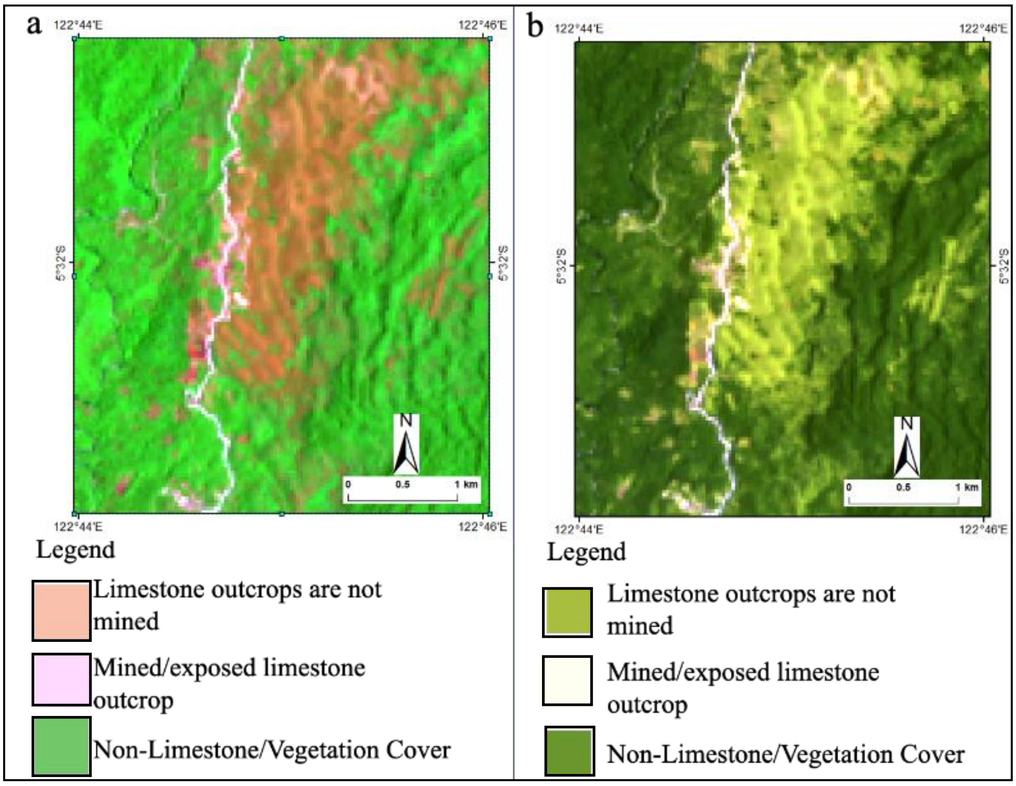

Fig. 3. (a) Colour composite results of RGB: 753; (b) RGB: 762 Landsat 8 images

The specific RGB combinations 753 and 762 are not mentioned in the provided papers, but Landsat 8 OLI band was effective in discriminating various rock unit and associated mineral deposits. Additionally, band ratios such as 4/2, 6/7, and 6/5 were found to be useful for identifying granitoids and gneisses bearing iron and hydroxyl minerals. The identification of the color of limestone outcrops based on band ratios and color composites shows varied and significant color differences from non-limestone outcrops. Apart from being based on band ratios and color composites, spectral identification in Landsat 8 images was performed to show the spectral characteristics of each band of Landsat 8 images. The spectrum has high reflectance in band 6 (1.57-1.65 µm) and low reflections in band 7 (2.11-2.29 µm) in unmined limestone (Fig. 4a) and mined limestone (Fig. 4b). The vegetation or non-limestone showed the opposite reflectance, that is, low in band 6 (Fig. 4c).

3.3. Normalized Differenced Vegetation Index

Since the 1970s, researchers have employed the NDVI to extract vegetation index values from remote sensing data. Many scientists have utilized NDVI with the increasing availability of satellite and Unmanned Aerial Vehicle (UAV) remote sensing imagery (Venkata et al., 2022). Vegetated and non-vegetated areas can be distinguished using NDVI (Somayajula et al., 2021). NDVI values between -1 and +1. Water bodies had negative NDVI values (values close to -1). Values close to zero (-0.1 to 0.1) indicate barren sand and rock. NDVI values from 0.1 to 0.2 indicate the surface of the land or open land. Low NDVI with a value of 0.2-0.4 indicates bushes, grasslands, and NDVI values between 0.6 to 1.0 indicate dense vegetation.

NDVI analysis of operational limestone quarries revealed values ranging from -0.1 to 0.05. The likelihood of limestone presence increases as NDVI values decrease, corresponding to the naturally white appearance of the mineral (Venkata et al., 2022). The NDVI threshold value for determining active mining limits ranges from -0.1 to 0.05 (Kotaridis et al., 2020). The formula used to calculate the NDVI value through the red (red) and near-infrared (NIR) bands from the Landsat 8 spectral is as follows:

$$\text{NDVI=Indeks(NIR,Red)}=\frac{\text{NIR-Red}}{\text{NIR+Red}}=\frac{(B5-B4)}{(B5+B4)}, \quad (1)$$

The NDVI values in this research area show several types of land cover, namely, water bodies, open land, vegetated land, and limestone. Unmined limestone outcrops show a value of 0.3-0.5, mined or exposed limestone outcrops show an NDVI value of 0.1-0.2 and non-limestone or vegetation NDVI values of 0.6-1.0 (Fig. 5). Limestone areas that have been mined or exposed show low NDVI values, which shows that the land or vegetation cover has been disturbed by mining activities.

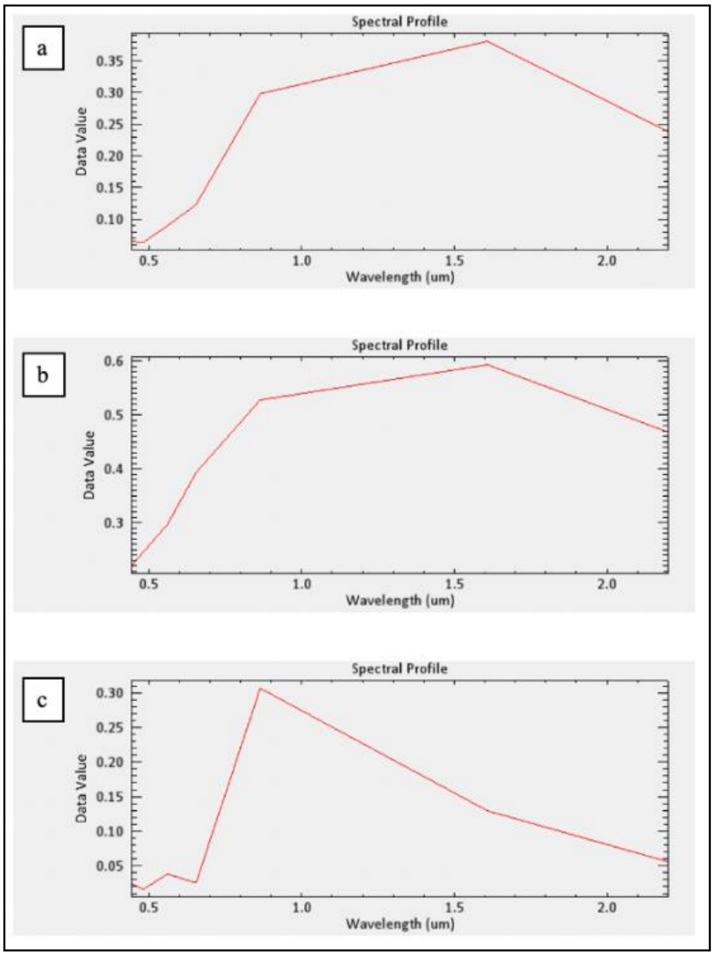

Fig. 4. (a) Spectral curve of unmined limestone; (b) spectral curve of mined or exposed limestone; (c) spectral curve of vegetation/non-limestone

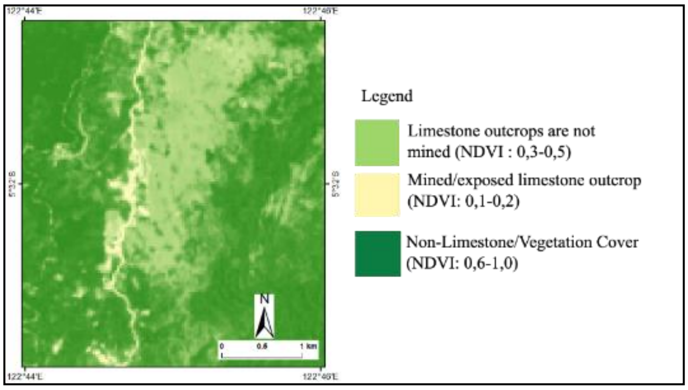

Fig. 5. NDVI of the study area

3.4. Field and Laboratory Studies

Field data were collected to validate the capability of Landsat 8 imagery to interpret and distribute limestone. Five locations were spread across the research area. ST.01 (Fig. 6a and 6b) is a limestone outcrop on the side of the road, based on observations in the field of greyish-white limestone. The thickness of the limestone at location ST. 01 was approximately 2-5 meters along the roadside (Fig. 6a). ST.02 (Fig. 6c and 6d) and ST.03 (Fig. 6e and 6f) are former community mining locations or limestone mining openings. The limestone at ST.02 (Fig. 6d) has the same color, namely, brownish white, and the exposed limestone is 2-5 meters thick. At ST.03 the limestone is up to 20 meters thick and has a brownish white colour (Fig. 6f).

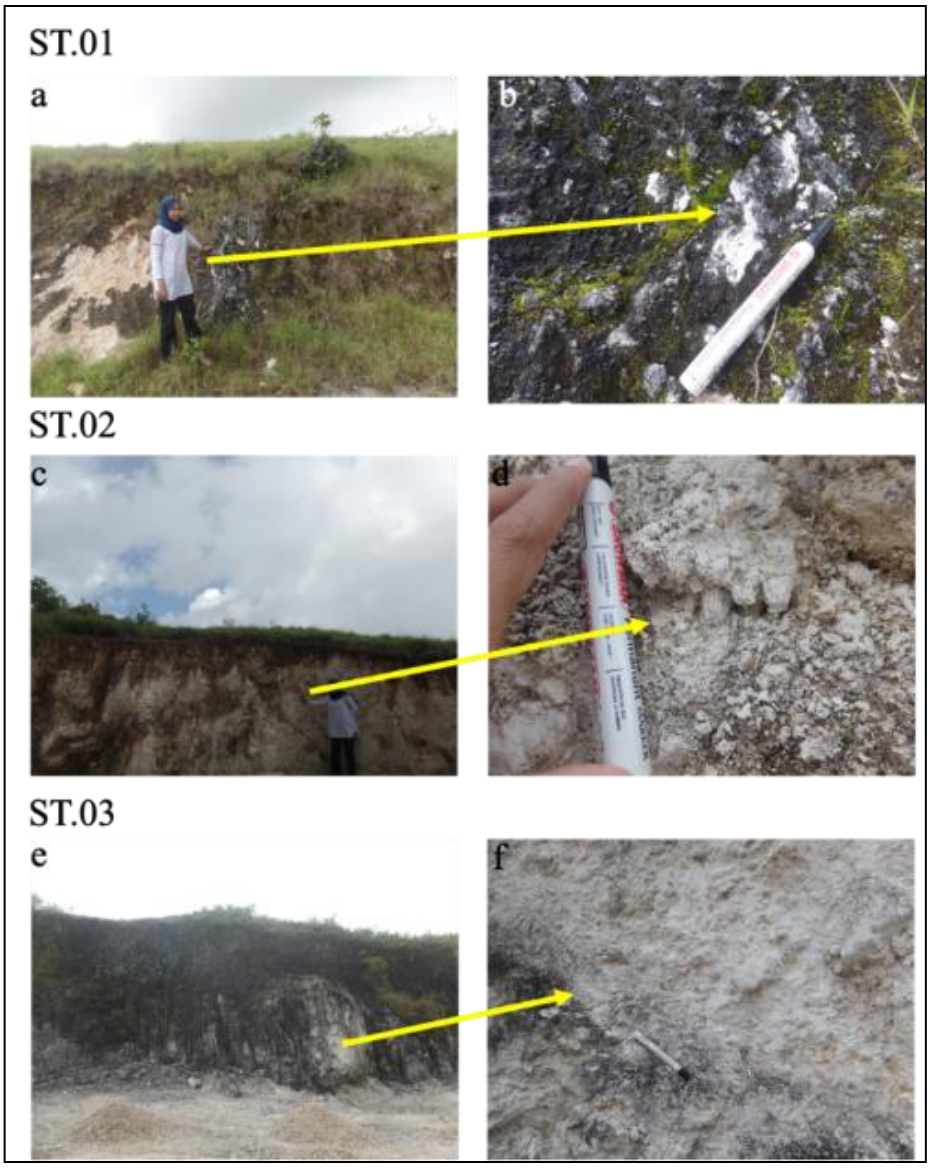

Fig. 6. Limestone outcrops in the study area ST 01 unmined limestone location, ST 02 and ST 03 mined limestone locations

ST.04 (Fig. 7a and 7b) is a former limestone mine and the land used to extract heaped rock for building materials. The limestone outcrop at ST.04 is up to 15 m thick and brownish white in colour. At ST.05 (Fig. 7c and 7d), the limestone outcrop is located at a limestone mine operated by the local community. The opening of the limestone mine contained rock excavation holes. The limestone outcrop at ST.05 is grayish-brown-white with a thickness of 10-20 meters.

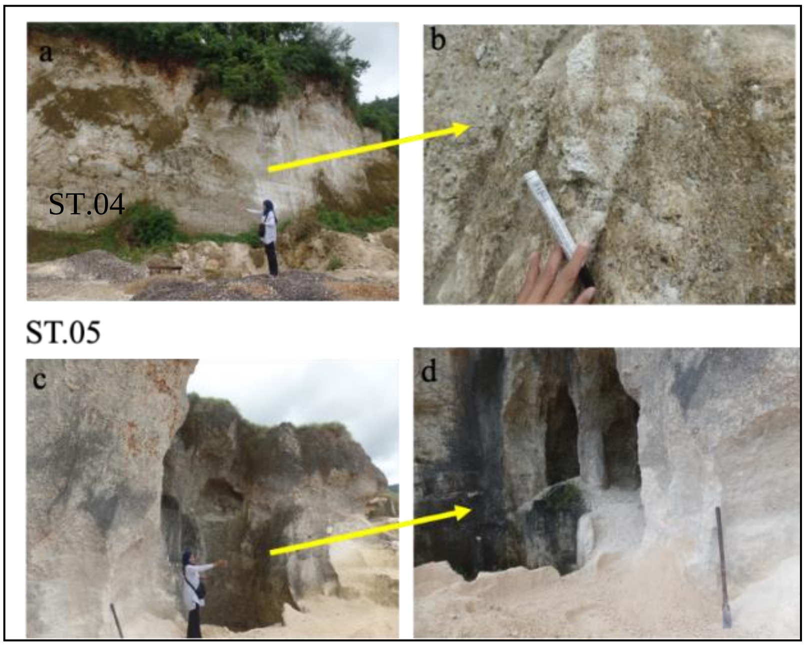

Fig. 7. Limestone outcrops in the ST 04 and ST 05 research areas at the mined limestone location

The laboratory analysis used in this study was XRF analysis to determine the chemical content of each sample. For XRF the rock samples were ground and crushed to a powder (Alrawi et al., 2023; Salih et al., 2023). Table 2 shows the XRF results.

Table 2. Results of XRF analysis of limestone in the study area

No	Location	Minerals	Quantitative (%)
1	ST.01	CaO	98,36
		K_2O	0,66
		Ru_2O	0,45
		Fe_2O_3	0,41
		Ag_2O	0,05
		SrO	0,03
		CuO	0,02
2	ST.02	CaO	99,30
		Ru_2O	0,43
		Fe_2O_3	0,19
		Ag_2O	0,03
		CuO	0,02
3	ST.03	CaO	99,40
		Ru_2O	0,44
		Ag_2O	0,07
		4SrO	0,04
		CuO	0,02
4	ST.04	CaO	98,80
		K_2O	0,68
		Ru_2O	0,42
		Ag_2O	0,05
		CuO	0,02
5	ST.05	CaO	98,94
		K_2O	0,42
		Fe_2O_3	0,61
		CuO	0,02

The limestone sample analysis showed the presence of a high CaO content (>97%). The limestone is identified as coral seamount rock with a number of fossil fragments, and the limestone shows the presence of coral reefs rich in calcite minerals with fossil skeletons observed in limestone from shallow marine facies. XRF analysis of the samples confirmed reef limestone mineralization.

4. Conclusions

This research uses Landsat 8 to identify the distribution and potential of limestone in South Buton, Southeast Sulawesi Province, using the band ratio, color composite, and NDVI methods. The research results based on remote sensing data from Landsat 8 imagery divided the characteristics of limestone into three types: unmined limestone, mined limestone, and non-limestone. The color characteristics displayed from the band ratio and color composite results show significant color differences from limestone outcrops in the study area. The NDVI method shows land or areas that are disturbed by limestone mining activities, so the NDVI value is low because the vegetation value is low or the vegetation cover is disturbed due to mining activities in the research area. The spectral curve of each Landsat 8 image band showed high reflectance in band 6 for limestone and low reflectance in band 6 for non-limestone.

The results of the XRF analysis of limestone samples from the research area reveal a high CaO content, averaging 98.96 which indicates a dominant calcite mineral composition. This finding is consistent with the geological characteristics of limestone formations in the region.

References

Abdelmalik, K.W., 2020. Landsat 8: Utilizing sensitive response bands concept for image processing and mapping of basalts. The Egyptian Journal of Remote Sensing and Space Science, 23(3), 263–274, https://doi.org/10.1016/J.EJRS.2019.04.004

Alrawi, S.S., Kadhim, L.S., Al-Hadaithy, A.A., 2023. Mineralogy and geochemistry of Anah and Euphrates formations and their suitability for Portland cement and noora industry at Al-Baghdadi and Haditha areas, western Iraq. Iraqi Geological Journal, 56(2D), 177-186. https://doi.org/10.46717/igj.56.2D.14ms-2023-10-20.

Amer, R., Kusky, T., Ghulam, A., 2010. Lithological mapping in the central eastern desert of Egypt using ASTER data. Journal of African Earth Sciences, 56 (2–3), 75-82. https://doi.org/10.1016/j.jafrearsci.2009.06.004

Bedini, E., 2011. Mineral mapping in the Kap Simpson complex, central East Greenland, using HyMap and ASTER remote sensing data. Advances in Space Research, 47(1), 60-73. https://doi.org/10.1016/j.asr.2010.08.021

Benaissi, L., Tarek, A., Tobi, A., Ibouh, H., Zaid, K., Elamari, K., Hibti, M., 2022. Geological mapping and mining prospecting in the Aouli inlier (Eastern Meseta, Morocco) based on remote sensing and geographic information systems (GIS). China Geology, 5(4), 614–625, https://doi.org/10.31035/CG2022035`

Bety, A.K.S., 2022. Discrimination different lithological units using a remote sensing application: A case study in the Dokan Area, Kurdistan Region, Iraq. Journal of Water and Land Development, 55, 109–114. https://doi.org/10.24425/jwld.2022.142312

Bety, A.M., Al-Kubaisi, M.S., 2024. The application of remote sensing techniques for identification of gypsum rocks in the Qara Darbandi Anticline, Kurdistan Region of Iraq. Iraqi Geological Journal, 57(1E), 308-322. https://doi.org/10.46717/igj.57.1E.20ms-2024-5-31

Crouvi, O., Ben-Dor, E., Beyth, M., Avigad, D., Amit, R., 2006. Quantitative mapping of arid alluvial fan surfaces using field spectrometer and hyperspectral remote sensing. Remote Sensing of Environment, 104(1), 103-117. https://doi.org/10.1016/j.rse.2006.05.004

Di Tommaso, I., Rubinstein, N., 2007. Hydrothermal alteration mapping using ASTER data in the Infiernillo porphyry deposit, Argentina. Ore Geology Reviews, 32 (1–2), 275-290. https://doi.org/10.1016/j.oregeorev.2006.05.004

Ding, C., Liu, X., Liu, W., Liu, M., Li, Y., 2014. Mafic–ultramafic and quartz-rich rock indices deduced from ASTER thermal infrared data using a linear approximation to the Planck function. Ore Geology Reviews, 60, 161-173. https://doi.org/10.1016/j.oregeorev.2014.01.005.

Gad, S., Kusky, T., 2006. Lithological mapping in the Eastern Desert of Egypt, the Barramiya area, using Landsat thematic mapper (TM). Journal of African Earth Sciences, 44(2), 196–202, https://doi.org/10.1016/J.JAFREARSCI.2005.10.014

Heriyansyah, A.F., Chalik, C.A., Wakila, M.H., Harwan, Husain, J.R., F, F., 2022. Identifikasi Sebaran Batugamping Menggunakan Data Citra Landsat 8 Di Pulau Buton Bagian Selatan. Jurnal Geomine, 10(1), 59–74, https://doi.org/10.33536/JG.V10I4.985

Hunt, G.R., 1977. Spectral signatures of particulate minerals in the visible and near infrared. Geophysics, 42(3), 501–513, https://doi.org/10.1190/1.1440721

Kotaridis, I., Lazaridou, M., 2020. Delineation of open-pit mining boundaries on multispectral imagery. Remote Sensing, 1-15. https://doi.org/10.5772/INTECHOPEN.94120

Lu, Y., Yang, C., He, R., 2022. Towards lithology mapping in semi-arid areas using time-series Landsat-8 data. Ore Geology Reviews, 150, 105163. https://doi.org/10.1016/J.OREGEOREV.2022.105163

Moghtaderi, A., Moore, F., Mohammadzadeh, A., 2007. The application of advanced space-borne thermal emission and reflection (ASTER) radiometer data in the detection of alteration in the Chadormalu paleocrater, Bafq region, Central Iran. Journal of Asian Earth Sciences, 30 (2), 238-252. https://doi.org/10.1016/j.jseaes.2006.09.004

Muchsin, F., Fibriawati, L., Pradhono, K.A., 2018. Model Koreksi Atmosfer Citra Landsat-7 (Atmospheric Correction Models Of Landsat-7 Imagery). Jurnal Penginderaan Jauh dan Pengolahan Data Citra Digital, 14(2), https://doi.org/10.30536/J.PJPDCD.1017.V14.A2595

Osinowo, O.O., Gomy, A., Isseini, M., 2021. Mapping hydrothermal alteration mineral deposits from Landsat 8 satellite data in Pala, Mayo Kebbi Region, southwestern Chad. Scientific African, 11, e00687. https://doi.org/10.1016/J.SCIAF.2020.E00687

Ourhzif, Z., Algouti, A., Algouti, A., Hadach, F., 2019. Lithological mapping using landsat 8 oli and aster multispectral data in imini-ounilla district south high atlas of marrakech. In International Archives of the Photogrammetry, Remote Sensing and Spatial Information Sciences - ISPRS Archives., https://doi.org/10.5194/isprs-archives-XLII-2-W13-1255-2019

Pour, A.B., Hashim, M., 2011. Identification of hydrothermal alteration minerals for exploring of porphyry copper deposit using ASTER data, SE Iran. Journal of Asian Earth Sciences, 42 (6), 1309-1323. https://doi.org/10.1016/j.jseaes.2011.07.017

Pour, A.B., Hashim, M., 2023. The application of Landsat-8 OLI/TIRS data for geological mapping: a case study from SE Iran. Retrieved February 17, 2023 from http://earthexplorer.usgs.gov

Pour, A.B., Park, Y., Park, T.Y.S., Hong, J.K., Hashim, M., Woo, J., Ayoobi, I., 2018. Regional geology mapping using satellite-based remote sensing approach in Northern Victoria Land, Antarctica. Polar Science, 16, 23–46, https://doi.org/10.1016/J.POLAR.2018.02.004

Rockwell, B.W., Hofstra, A.H., 2008. Identification of quartz and carbonate minerals across northern Nevada using aster thermal infrared emissivity data-implications for geologic mapping and mineral resource investigations in well-studied and frontier areas. Geosphere, 4 (1), 218–246. https://doi.org/10.1130/GES00126.1

Sabins, F.F., 1999. Remote sensing for mineral exploration. Ore Geology Reviews, 14 (3–4), 157-183. https://doi.org/10.1016/S0169-1368(99)00007-4

Salih, N.M., Thannoun, R.Gh., 2023. Hydrocarbon seepage detection by integrating remotely sensed and geochemical data: scanning the lithological alteration. Arabian Journal of Geosciences, 16, 11209. https://doi.org/10.1007/s12517-023-11209-3

Sikumbang, N., 1995. Peta geologi lembar Buton, Sulawesi Tenggara Geological map of the Buton sheet, Southeast Sulawesi.

Somayajula, V.K.A., Ghai, D., Kumar, S., 2021. Land use/land cover change analysis using NDVI, PCA. 5th International Conference on Computing Methodologies and Communication (ICCMC), 849–855, https://doi.org/10.1109/ICCMC51019.2021.9418025

Soni, A.K., Nema, P., 2021. About Limestone. Materials Horizons: From Nature to Nanomaterials, 1–16, https://doi.org/10.1007/978-981-16-3560-1_1

Venkata, S.C., Umamaheswara, R.G., Usha, R.N., 2022. Delineation and evaluation of the captive limestone mining area change and its influence on the environment using multispectral satellite images for industrial long-term sustainability. Cleaner Engineering and Technology, 10, 100551, https://doi.org/10.1016/J.CLET.2022.100551

Wei, J., Liu, X., Liu, J., 2016. Integrating textural and spectral features to classify silicate-bearing rocks using Landsat 8 data. Applied Sciences, 6(10), 283, https://doi.org/10.3390/APP6100283